Journal of Marine Research, 56, 349–374, 1998

On the parameterization of eddy transfer, Part II: Tests with a channel model

by Peter D. Killworth[1]

ABSTRACT

In Part I of this paper (Killworth, 1997), a new eddy parameterization scheme was presented. Here, the scheme is tested by comparing its predictions with those of multi-year averages from an eddy-resolving channel model. Its accuracy is similar to that of a tuned version of previous schemes. However, a tuned version of the new parameterization can reproduce both the long-term average of the eddy-resolving solution as well as the initial slumping of a narrow front. Both tuned schemes reproduced the bolus transport well. The new parameterization reproduces the observed feature that the diffusivity is maximal at mid-depth and minimal at surface and floor.

1. Introduction

Until computing platforms are sufficiently fast so that truly eddy-resolving ocean models can be run in climate mode, deductions about climate change will have to be made from models which contain no eddy-permitting dynamics. To avoid these difficulties, eddy parameterizations will have to be employed for the foreseeable future. Since there are numerous mechanisms which produce eddies, and equally numerous ocean responses to the presence of eddies, a single parameterization is singularly unlikely to be representative of the wide spectrum of eddies.

Much attention has focused on eddies produced by the release of available potential energy; i.e., by baroclinic instability, because such eddies pervade the world ocean. In Part I of this paper, Killworth (1997, hereafter K97) produced a form of parameterization by considering slowly varying linear baroclinic instability. This form was similar to, but differed significantly in several respects from, that suggested by Gent and McWilliams (1990). In particular, the eddy diffusivity employed varied spatially both horizontally and vertically, with maxima at mid-depth several times larger than values at surface or floor.

The purpose of this paper is to test the parameterization against the Gent and McWilliams scheme in a channel model. Section 2 briefly describes the model, and Section 3 shows the results. Section 4 compares bolus transports from the channel model with those predicted from the parameterizations.

1. Southampton Oceanography Centre, Empress Dock, Southampton SO14 3ZH, United Kingdom.

2. The channel model

The K97 parameterization, in two-dimensional mode, was tested and compared with the Gent and McWilliams (1990) formulation, using an eddy-resolving channel model. A previous test of this type was made by Visbeck *et al.* (1997). However, most of the tests they employed were initial value problems; the parameterizations discussed here are more relevant to steady-state situations with well-developed instabilities than to initially growing modes. Accordingly, the model used here was run over a complete growth and decay cycle.

Channel models have advantages and disadvantages for parameterization tests. They permit a test of schemes in one lateral direction only, and can be forced (as here) to a solution which has no areas of static instability, where any bolus-based parameterization breaks down. However, they also suffer from atypical dynamics in the along-channel direction, formally requiring parameterization of the Reynolds' stresses to produce an accurate simulation. Marshall (1981) discusses this problem. The high along-channel velocities produced also permit barotropic instability, for which most extant parameterizations are not designed.

The channel was oriented east-west (denoted by x, with velocity u) over a longitude range of 2.6°, which is sufficiently wide to contain three wavelengths of the fastest growing linear mode of the initial configuration. The channel occupied a latitudinal (denoted by y, with velocity v) extent of 5.2°, centered on 30N. Its depth (denoted by z, with velocity w) was 300 m; this shallow depth was chosen because the configuration had previously been used for other purposes. The model used the MOMA code (a variant of the GFDL MOM code, Webb, 1996) with tracer advection by the QUICK scheme (Farrow and Stevens, 1995), in a fully spherical configuration. The grid spacings used were 5 m vertically and 0.2° east-west, 0.18° north-south (giving a spacing of 2 km horizontally); the deformation radius, about 10 km, was well resolved by this choice. All walls are insulating; there is no slip on the north-south walls, and no stress conditions at surface and floor. Numerical eddy coefficients were fairly normal for such resolution: viscous terms were 50 $m^2\ s^{-1}$ horizontally and 5 vertically; diffusion terms were 10 $m^2\ s^{-1}$ horizontally and 1 vertically. Such a run is fairly viscous, but has the virtue of equilibrating with realistic currents. Another option would have been biharmonic terms (but the QUICK scheme was not available for that case).

Initially the channel was occupied by a narrow temperature front (salinity was uniform, with a linear equation of state) of the form used by Samelson (1993), although the channel here is much wider either than the front or than the width, the front would slump to following initial baroclinic instability. There was a small seeding of the maximum linear disturbance added at time zero. Eddies build up rapidly on this front, producing significant distortions within 24 days; Figure 1 gives a typical example of the behavior. Left to itself, the release of baroclinic energy would run the system down, eventually producing the flat isopycnals seen as the end result in Gent *et al.* (1995). To prevent this, energy was

re-introduced by a strong relaxation of the temperature field back to its initial distribution in 30 grid points at the north and south boundaries. (The relaxation is sufficiently strong that the boundary condition is effectively that of a given temperature on the vertical walls.) This condition yields a long time behavior akin to that studied by Simmons and Hoskins (1978), where the energy lost from the baroclinic field was slowly returned by solar heating. As noted above, the relaxation employed here has the advantage that a statistically steady state can exist with all the fluid stably stratified, thus avoiding choices about parameterizations in neutrally stable or unstable regions.

The long-time behavior of the available potential energy (computed correctly, using a redistribution method of Nurser, private communication) is shown in Figure 2. Following the initial slump of the front (to almost the value relevant for a temperature field linearly interpolated between the two vertical boundaries), and concomitant release of potential energy, over a period of several years, the available potential energy increases slowly as the front is re-created by the boundary forcing. At the end of the period shown, the front begins a second collapse. Computer restrictions prevented following of the cycle further, but there is no reason to doubt that another collapse and re-creation of potential energy will occur. However, there is no direct proof that the second cycle will parallel the first since it starts from a different configuration. There is, simply, no good time to halt the experiment; were additional computer time available, a gyre-scale calculation would probably be preferred to an extension of the experiment here.

In what follows, the channel model will be described by zonal averages (along-channel) and time averages over the time period 300 to 2950 days (i.e., over one complete recovery cycle, about 7.25 years). Such a description is hardly statistically reliable, but gives a good guide to the behavior of the system.

Figures 3 and 4 show the average temperature and zonal velocity respectively (the mean meridional and vertical velocities are negligible). The temperature field displays two fronts, with a region of flatter isopycnals between them. There is evidence of upwelling against the northern region of relaxation, which has led to isopycnals raised above their relaxed level. The resulting zonal velocity is dominated by barotropic flow.[2] The velocity is eastward near both boundaries, and westward in the center of the channel. The jet is much wider than its original configuration. The vertical (baroclinic) shear is much weaker than the barotropic flow, and the purely baroclinic part of the zonal flow is shown in Figure 4b. As expected from the density forcing applied, the baroclinic flow is predominantly eastward at the surface and westward at depth, though there are deviations from this near the southern boundary where the baroclinic flow returns to eastward at depth. Even with the long-time average, frontal structure remains evident. The zonal velocity is accurately in geostrophic balance.

2. With hindsight, it would have been preferable to have applied a bottom friction to damp the barotropic zonal velocity.

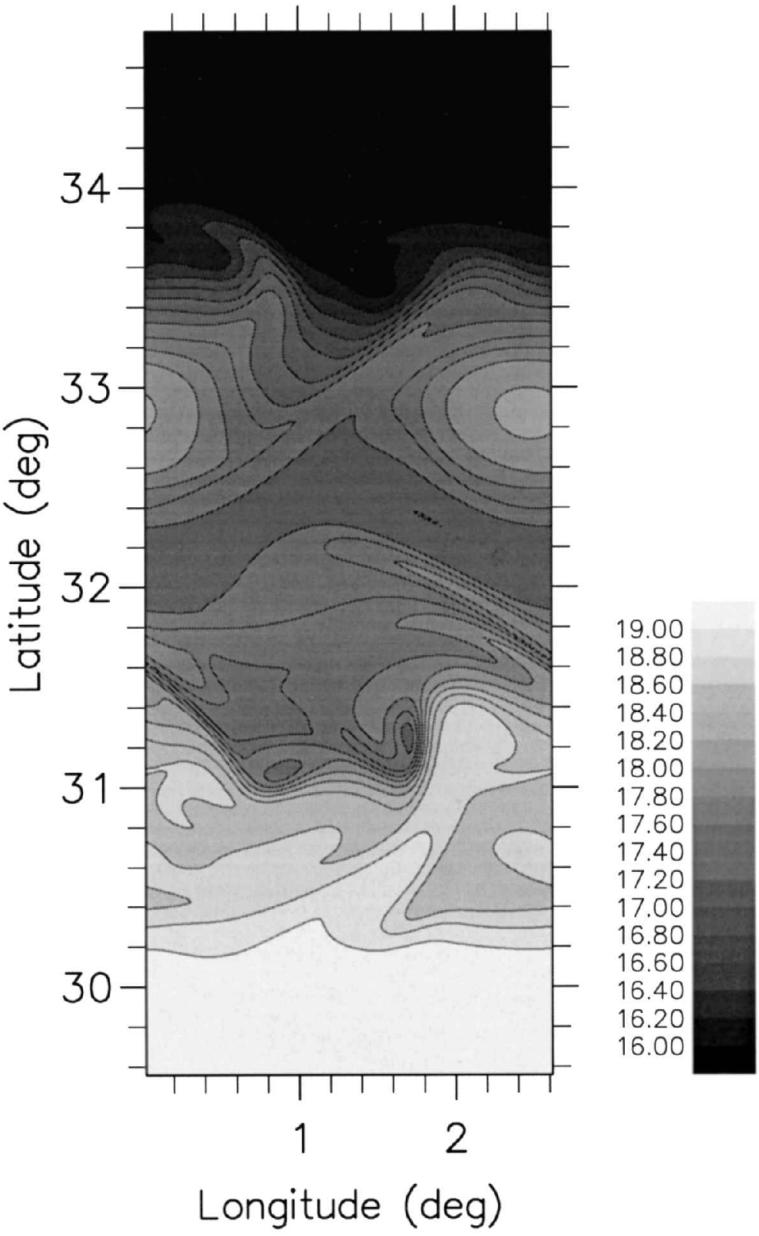

Figure 1. The surface temperature field early in the channel model integration, showing the gross distortions of the initial front. Contour interval 0.2°C, min/max values 15.9, 19.02°C.

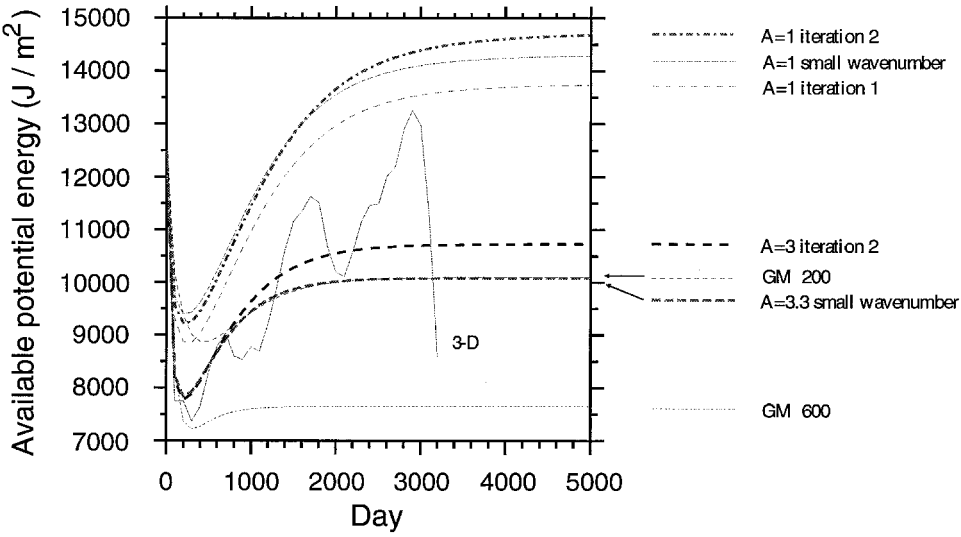

Figure 2. The long-time behavior of the available potential energy in the channel model (firm line). Also shown are the equivalent values for the two-dimensional model using the parameterizations indicated.

3. Tests using the channel model

Parameterization schemes were computed for comparison using a two-dimensional (vertical and north-south) model on a beta-plane, although the limited north-south extent of the model ($\beta L/f = 0.16$, where f is the Coriolis parameter, β its northward gradient, and L the north-south extent of the fluid) meant that the beta effect was small throughout. The equations are those for three dimensions, but with the zonal derivative set identically equal to zero. This has two important effects. First, as noted above, the Reynolds' stress term $(\overline{u'v'})_y$ in the zonal momentum equation is lost. This term appears to be responsible for the strong barotropic flow in the three-dimensional results, since no two-dimensional calculation has reproduced this effect. Second, the barotropic component of the u field has no effect on any other field in the two-dimensional model. To see this, note that u only occurs in one other equation, the north-south momentum equation, in the Coriolis term (because it has no advective role). But v has no vertical integral (mass continuity reads merely $v_y + w_z = 0$) so that the vertical average of u plays no part here. This leaves the u-momentum equation itself. Integrated w.r.t. depth, it gives

$$\frac{\partial}{\partial t}\int_{-H}^{0} u\,dz + \frac{\partial}{\partial y}\int_{-H}^{0} uv\,dz = A_H \frac{\partial^2}{\partial y^2}\int_{-H}^{0} u\,dz$$

where t is time, H is the (constant) depth, and A_H is the numerical friction coefficient. The nonlinear momentum term is made up of an integral of uv. The v field has no vertical

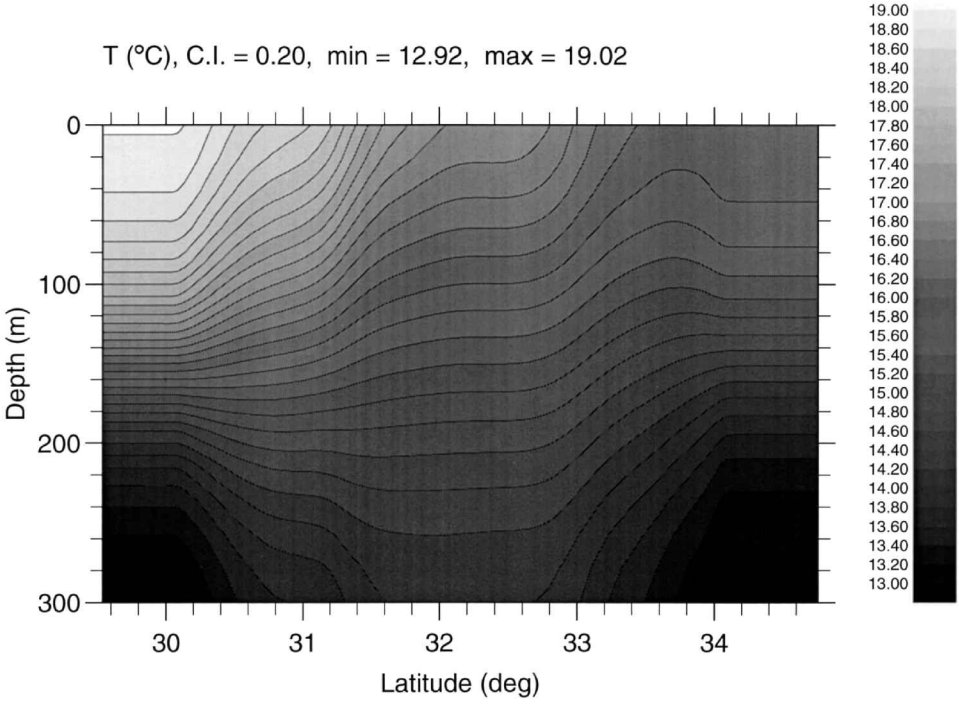

Figure 3. Zonal and time average of the temperature field in the channel model. Contour interval 0.2°C, min/max values 12.92, 19.02°C.

integral, and so the part involving the depth-averaged u field is identically zero; only the baroclinic part of u acts to avoid the spin-down of the barotropic flow by friction.

This means that the two-dimensional model cannot be expected to reproduce the barotropic part of the mean zonal velocity accurately[3]; but that this error is unlikely to cause many other difficulties—though clearly there will be small effects of the incorrect barotropic flow locally in the nonlinear terms. One could add in representations of the baroclinic eddy terms into the momentum equations (cf. Welander, 1973; Lee and Leach, 1996; Gent and McWilliams, 1996). Such actions would extend the test performed here from a (relatively simple) test of a pure parameterization in the density equation to a combined test of momentum and density parameterizations. This is not the intention here.[4]

Because the barotropic field is poorly reproduced, we shall refer only to the baroclinic u field in what follows, therefore.

3. This point has been confirmed directly by running the three-dimensional model with no downstream variation; the two-dimension solution (with no eddy parameterization) is reproduced. The two-dimensional calculations have almost no barotropic component.

4. Gent and McWilliams (1996) note that in general the changes to the flow induced by inclusion of eddy terms in the momentum equations will be small. The channel model considered here, with its limited sinks for momentum, is probably an exception.

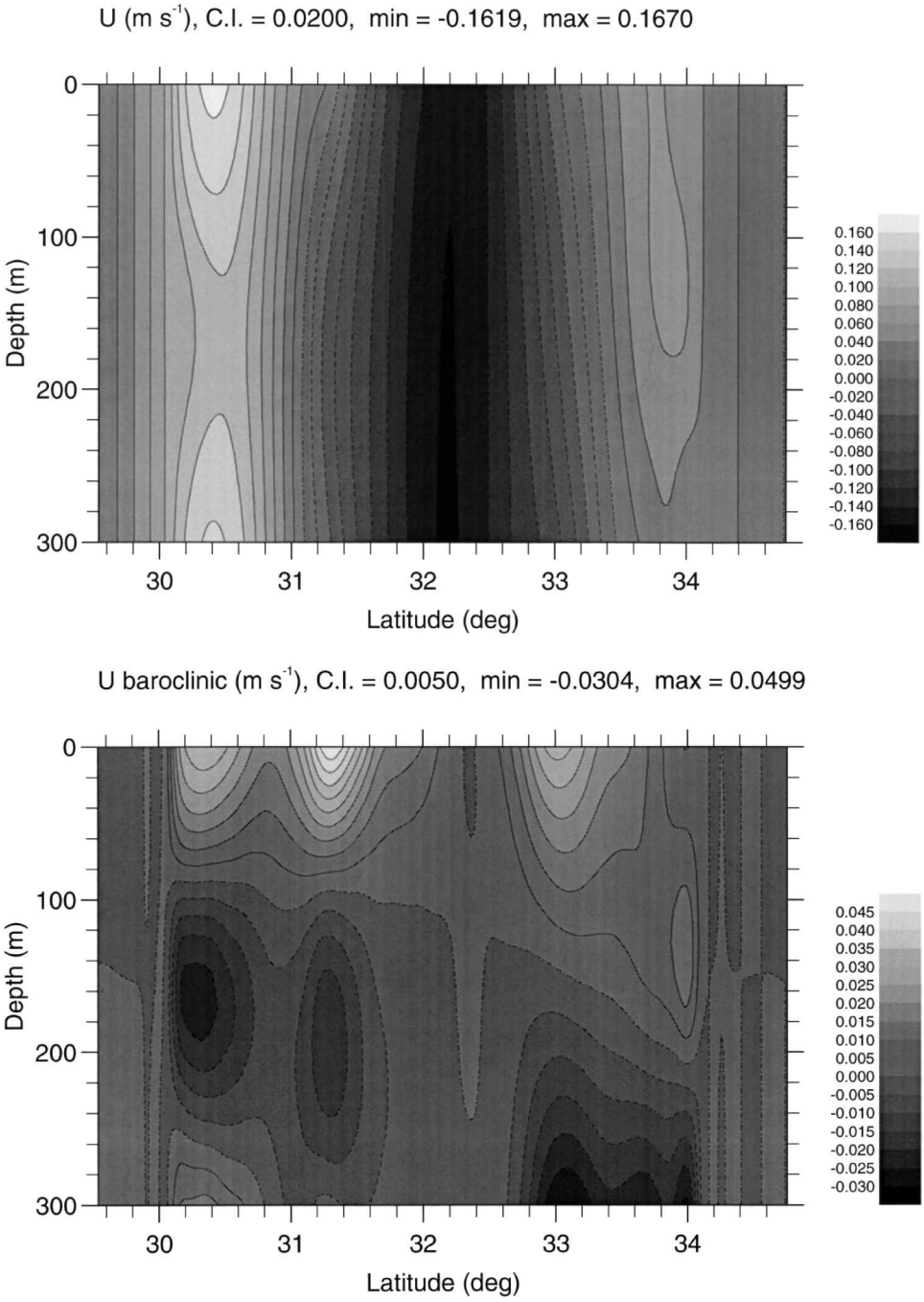

Figure 4. (a) Zonal and time average of the zonal velocity in the channel model. Contour interval 0.02 m s^{-1}, min/max values -0.162, 0.167 m s^{-1}. (b) The baroclinic part of the zonal velocity. Contour interval 0.005 m s^{-1}; min/max values -0.0304, 0.0499 m s^{-1}.

Four parameterization schemes were used (others examined being mentioned briefly):

(a) Gent and McWilliams (1990), hereafter GM, with a uniform diffusion coefficient of 600 $m^2\ s^{-1}$, chosen so that the release of available potential energy in the initial baroclinic disturbance matches that in the three-dimensional model;

(b) GM, but with a diffusion coefficient of 200 $m^2\ s^{-1}$, chosen so that the eventual release of available potential energy approximately matches that from the averaged three-dimensional model. Both (a) and (b) set the diffusion to zero in the top and bottom grid points, as required for conservation (see K97);

(c) the scheme discussed in this paper, using the small wavenumber expansion and a scaling coefficient A of unity (see Eq. (64) in K97);

(d) the scheme discussed here, using $A = 3.3$, with the linear scheme.

All the schemes reach a steady state after sufficient integration, and their steady solutions, after 5000 days, are used in what follows; the GM 600 scheme reaches a steady state much earlier than the other schemes. In the case of the new scheme, this is presumably due to the quadratic effect which the scheme has (the coefficient depends on density gradients and also acts on them; typically at the start of the integration the κ in the current scheme is several thousand $m^2\ s^{-1}$ at the sharp front; by the end of the integration it is a few hundred at most).

The methods used to examine the effectiveness of the schemes follow Harrison (1978) and Visbeck *et al.* (1997). These are (i) a direct correlation r between the time- and zonally-averaged three-dimensional (henceforth 3D) field and the parameterized two-dimensional equivalent, and (ii) a measure of explained variance (Visbeck *et al.*'s Eq. 25)

$$C = 1 - \frac{\sum_{y,z} (\tau_2 - \tau_3)^2}{\sum_{y,z} (\tau_3 - \overline{\tau}_3)^2}$$

where τ represents either temperature or zonal velocity, the suffix whether a 2- or 3-dimensional field is considered (the three-dimensional field being the zonal and time average above), and the bar representing a horizontal average. Both measures exclude the forcing region. However, as Visbeck *et al.* (1997) comment, the available potential energy (APE) is an excellent guide to the validity of the parameterizations, and to a large extent these other measures merely confirm that.

a. GM parameterization

Figure 5(a) shows the temperature using the GM parameterization with $\kappa = 600\ m^2\ s^{-1}$. Such a value is probably a little smaller than would be chosen for a basin scale of 5° (say $\kappa = 1000\ m^2\ s^{-1}$). The overall structure is similar to the averaged 3D temperature (a feature shared by all the schemes tested; the schemes are constrained by the setting of

temperature at north and south). The southward surface temperature gradient is too weak in this GM scheme; there is no evidence of the pseudo-upwelling near the northern boundary; and the dipping of the isopycnals near the floor in mid-channel is underestimated. A more stringent test is Figure 5(b), the baroclinic zonal velocity. Its strength is about half of the 3D case, reflecting the more slumped nature of the temperature field. Significantly, the baroclinic u field is everywhere positive at the surface and negative at the floor, so that the extra structure noted above is not present. Fig. 5(c) shows the bolus transport, with northward surface transport and southward return flow at depth apart from a reversed cell at the deep southern boundary.

The measures of accuracy of this simulation are given in Table 1. The temperature correlation is excellent (0.99), although only 74% of the spatial variance is accounted for. (From Fig. 2, the APE is grossly underestimated, so that the correlation is clearly a poor descriptor for testing purposes.) The equivalent figures for the baroclinic u field are 0.83 (correlation) and 0.40 (spatial variance). Both are less than the temperature values, suggesting that velocity is the better test of a parameterization in this particular configuration.

Figure 6 shows the contours from the GM scheme with $\kappa = 200\ m^2\ s^{-1}$. This would probably be deemed a small value by oceanographic standards, but is chosen to reproduce the APE level accurately. This tuned value, then, gives the best GM reproduction of the steady 3D results; but note from Figure 2 that it fails to estimate the initial loss of APE when the narrow front slumps. The temperature field is much better reproduced, though still too relaxed at the surface near the south; there is a good simulation of the pseudo-upwelling and the dipping of the isopycnals through the floor. The baroclinic u field has an accurate pattern, though still underestimating the minima and maxima. This is all reflected in the measures of accuracy: correlations and spatial variances of 0.99, 0.94 (temperature) and 0.85, 0.48 (velocity).

Thus the GM scheme can, with tuning, perform very well against the 3D results.

b. The new parameterization

Figure 7 shows contours using the new scheme, with nondimensional scaling parameter $A = 1$, and the small wavenumber formula. No attempt has been made to tune this coefficient, which is too small, as Figure 2 demonstrates. This borne out by the diagrams. The surface temperature gradient is quite tight against the southern boundary, as in the 3D run, and the pseudo-upwelling near the north, while reproduced by the method, has been overestimated. The dipping of deep isotherms is well reproduced, but overestimated. The baroclinic u field is still underestimated, although the minimum is accurately found. The region of eastward flow at the deep southern boundary is reproduced, as is the positive region at mid-depth at the northern boundary. The streamfunction for the bolus transport (Fig. 7 (c)) is very similar to the GM 200 streamfunction, both in pattern and in size. The diffusion coefficient κ which induces this field is shown in Figure 7 (d). Its maximum value

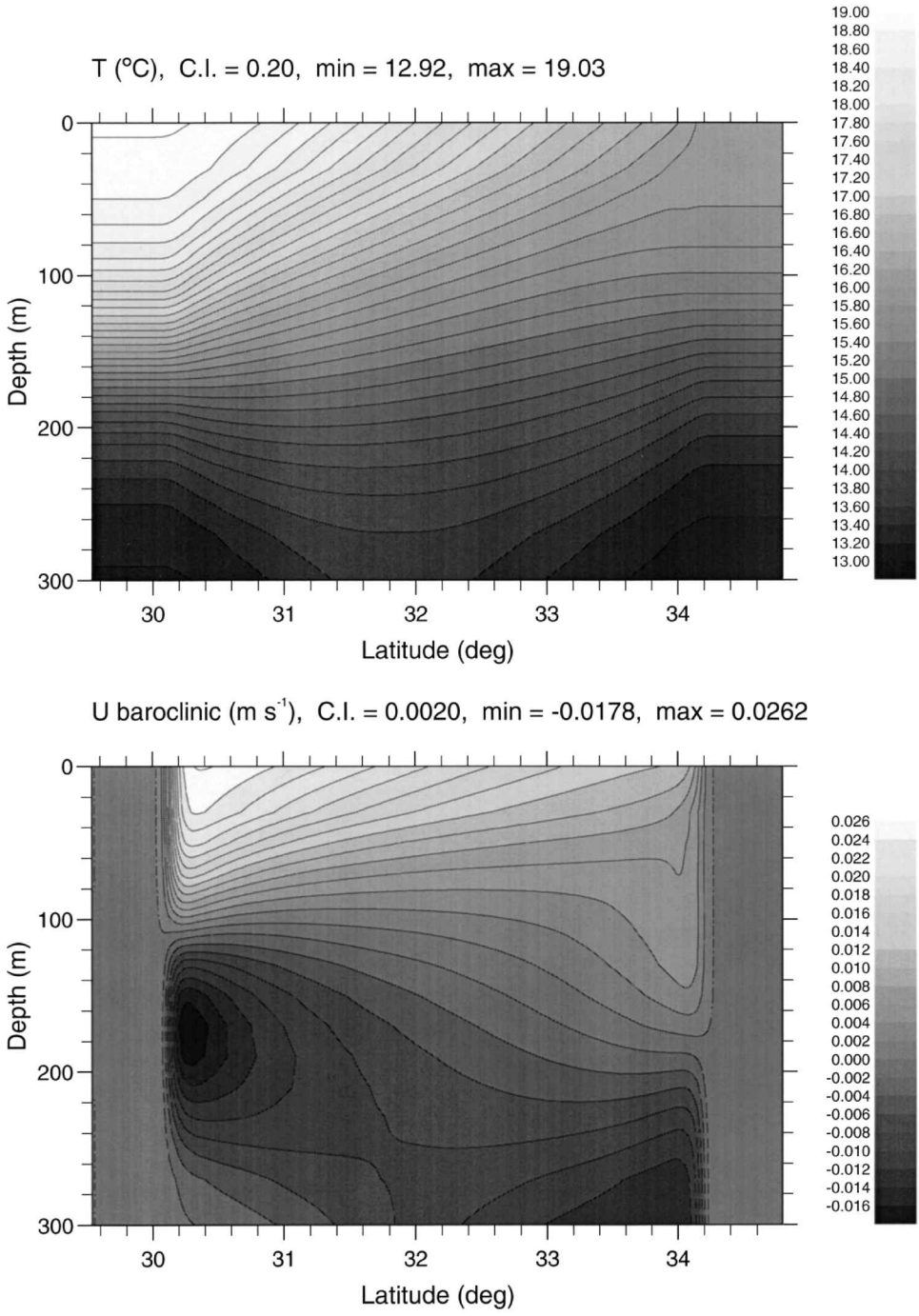

Figure 5. (a) Steady state solution for the temperature field using the GM scheme with $\kappa = 600\ m^2\ s^{-1}$. Contour interval 0.2°C, min/max values 12.92, 19.03°C. (b) The baroclinic part of the zonal velocity. Contour interval 0.002 m s^{-1}; min/max values −0.0178, 0.0262 m s^{-1}; (c) The streamfunction for the bolus transport; contour interval 0.05 $m^2\ s^{-1}$; min/max values −0.71, 0.31.

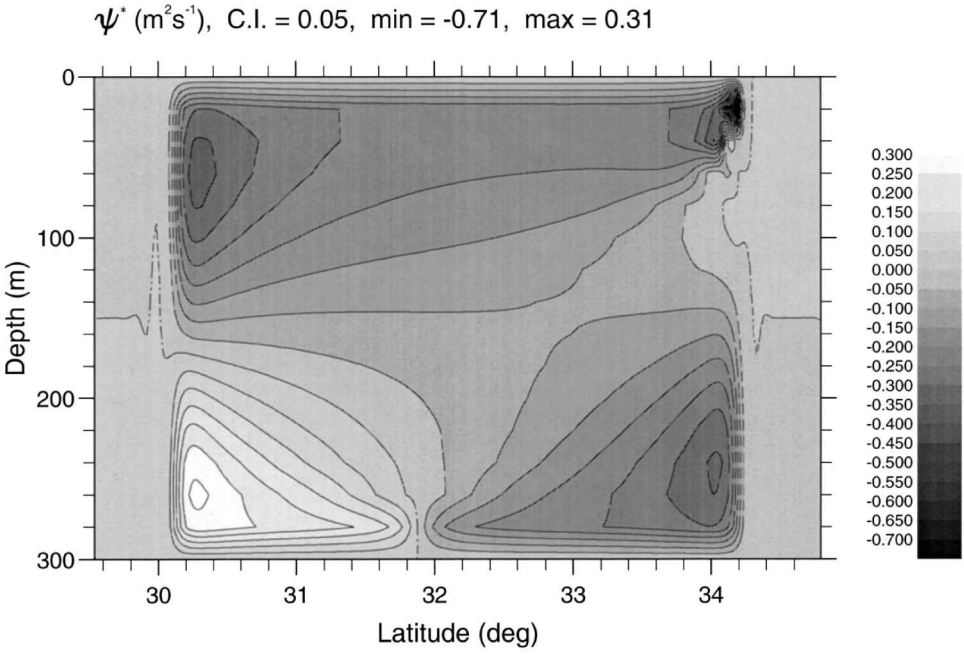

Fig. 5. (Continued)

is quite weak (about 200 $m^2\ s^{-1}$), with a maximum at mid-depth across the entire channel (and a secondary maximum at a lower depth near the southern boundary).

Table 1 shows that this simulation is slightly less accurate than the GM ($\kappa = 600$)equivalent (but recall that no attempt was made to tune the new scheme) insofar as the temperature field is concerned, with a correlation of 0.97 and 66% of the spatial variance accounted for. The velocity correlation was almost identical with the GM 600 case (0.82), although the spatial variance accounted for was less (0.23). The simulation was, of course, less accurate than the tuned GM 200 case.

Table 1.

	Temperature		Baroclinic velocity	
Method	Correlation	Spatial Variance	Correlation	Spatial Variance
GM, $\kappa = 600\ m^2\ s^{-1}$	0.99	0.74	0.82	0.40
GM, $\kappa = 200\ m^2\ s^{-1}$	0.99	0.94	0.85	0.48
New scheme, $A = 1$ small wavelength	0.97	0.67	0.82	0.23
New scheme, $A = 1$, iterative formula (once)	0.97	0.70	0.83	0.31
New scheme, $A = 1$, iterative formula (twice)	0.97	0.62	0.82	0.20
New scheme, $A = 3.3$, small wavelength	1.00	0.90	0.84	0.43
New scheme, $A = 3$, iterative formula (twice)	0.99	0.89	0.84	0.41

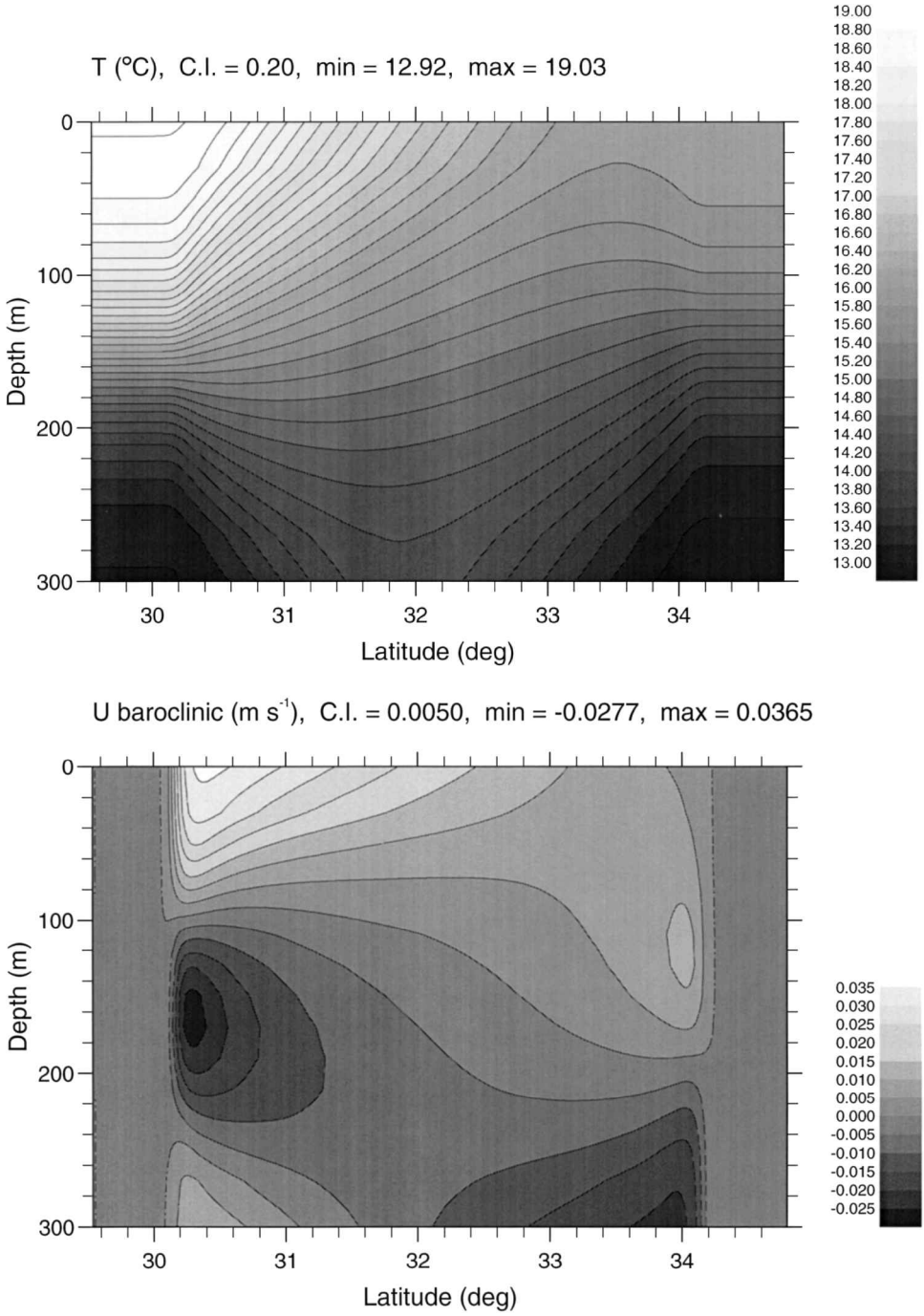

Figure 6. As for Figure 5, but using $\kappa = 200\ m^2\ s^{-1}$. (a) Contour interval 0.2°C, min/max values 12.92, 19.03°C. (b) The baroclinic part of the zonal velocity. Contour interval 0.005 m s^{-1}; min/max values -0.0277, 0.0365 m s^{-1}; (c) The streamfunction for the bolus transport; contour interval 0.02 $m^2\ s^{-1}$; min/max values -0.20, 0.18 $m^2\ s^{-1}$.

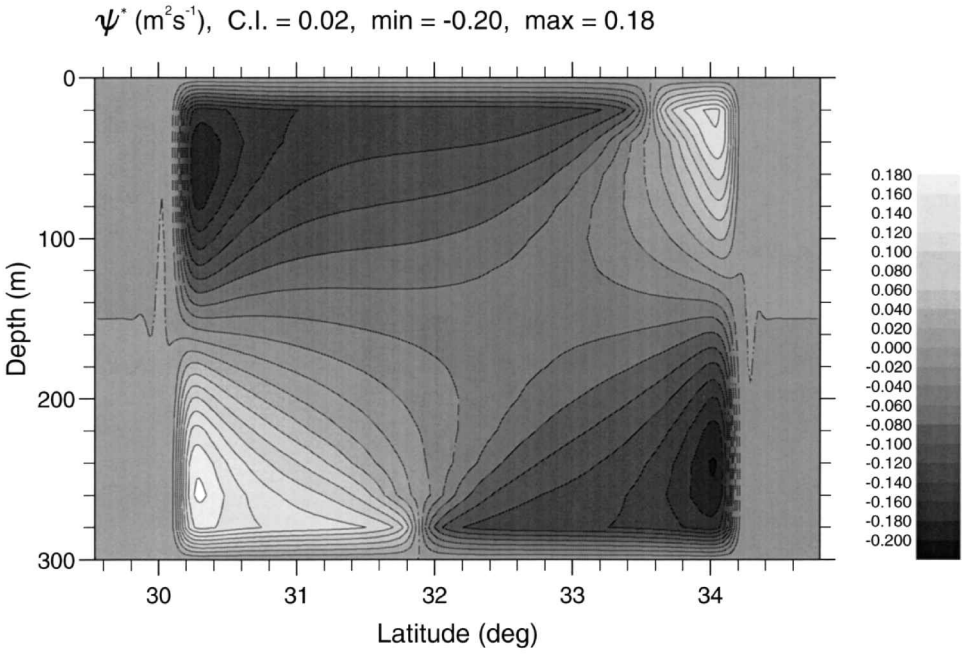

Fig. 6. (Continued)

Results using one iteration of the iterated scheme are visually identical. Since the effective mixing is smaller than the linearized case, as shown by the potential energy, the fit to the 3D case is improved by all estimates. Despite the indistinguishable results, the explained variance in the u field changes by 25% of its value. Results from the iterated method using two iterations are again visually identical to those previously, and are not shown here. Again as would be expected from the potential energy, the increased iterations have lessened the effective diffusivity and thus reduced the accuracy of the two-dimensional simulation on all counts. This is despite the fact that the temperature and velocity fields are most acceptable visually.

To provide a more reasonable test, the coefficient A was increased to 3.3, with the small wavenumber formula. Figure 2 shows that this reproduces both the long-term average APE, but also, remarkably, the initial slumping change in APE, unlike any GM simulation. This is presumably because the new scheme automatically modifies its diffusion value as the local shear changes. Figure 8 shows the solution in this case. Visually, the temperature field is more accurate than the GM 200 scheme, with the northern boundary particularly well reproduced (the correlation is 1.00, though the spatial variance accounted for is marginally less than the GM 200 value). The velocity field is predictably weaker than with a smaller coefficient; however, the two measures show improvements with this value of A. The bolus streamfunction is about 50% larger than the $A = 1$ case, and the diffusion κ is about 2.5 times larger than the $A = 1$ case, the differences being due to differences in the

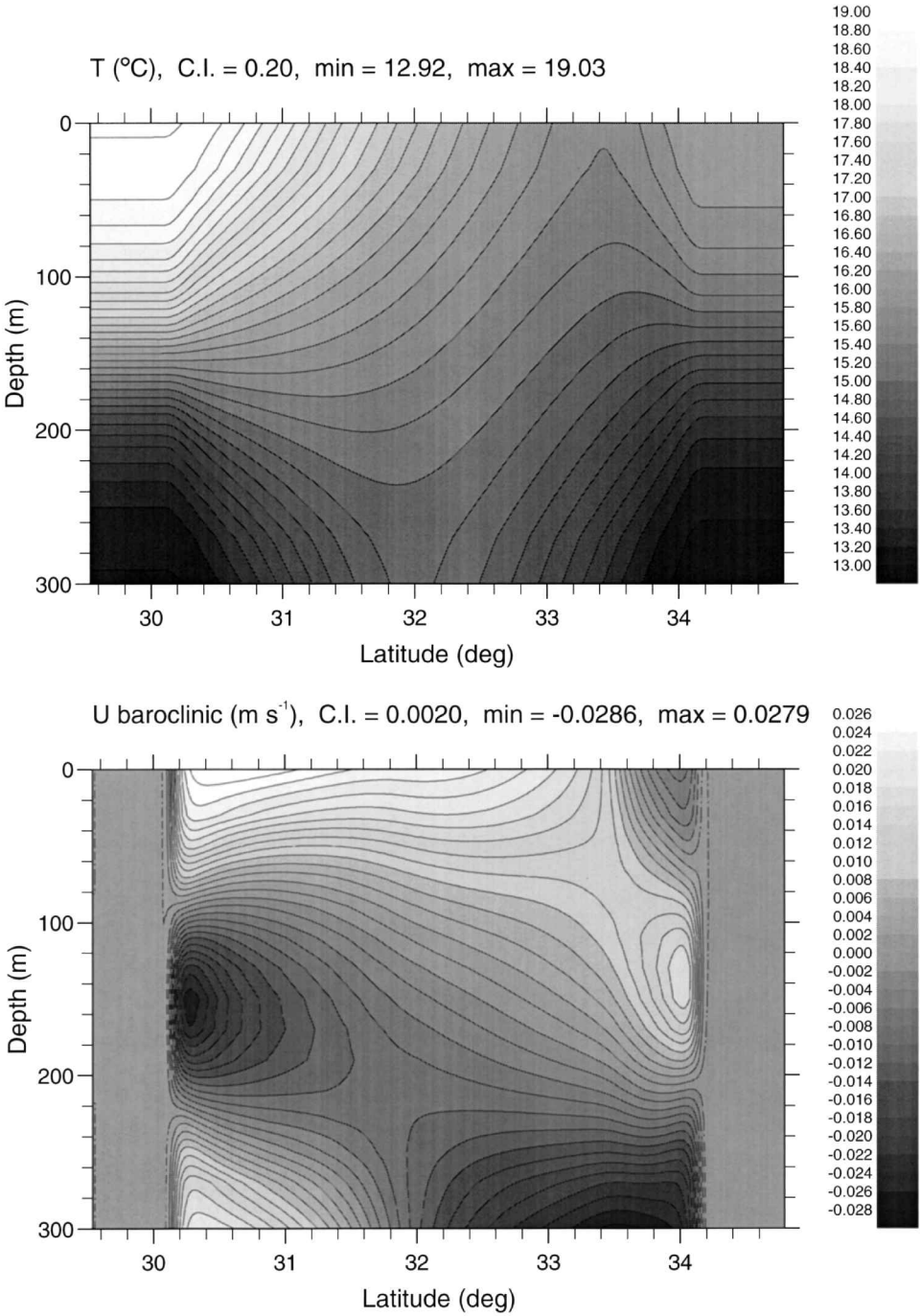

Figure 7. (a) Steady state solution for the temperature field using the new scheme with a coefficient $A = 1$, and the small wavenumber formula. Contour interval 0.2°C, min/max values 12.92, 19.03°C. (b) The baroclinic part of the zonal velocity. Contour interval 0.002 m s^{-1}; min/max values −0.0286, 0.0279 m s^{-1}; (c) The streamfunction for the bolus transport; contour interval 0.02 m^2 s^{-1}; min/max values −0.17, 0.15; (d) Distribution of the eddy diffusivity κ; contour interval 10 m^2 s^{-1}; max value 197 m^2 s^{-1}.

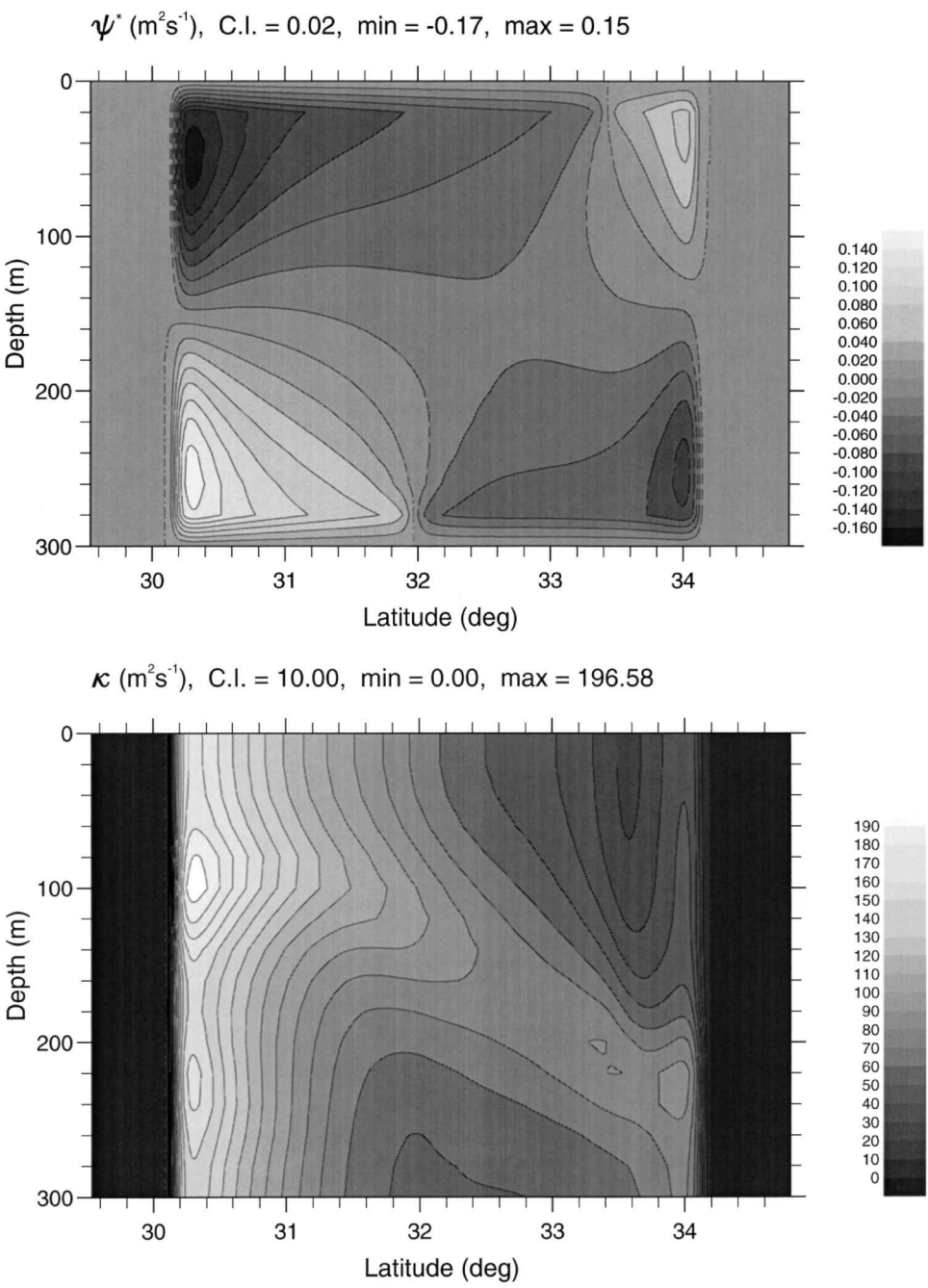

Fig. 7. (Continued)

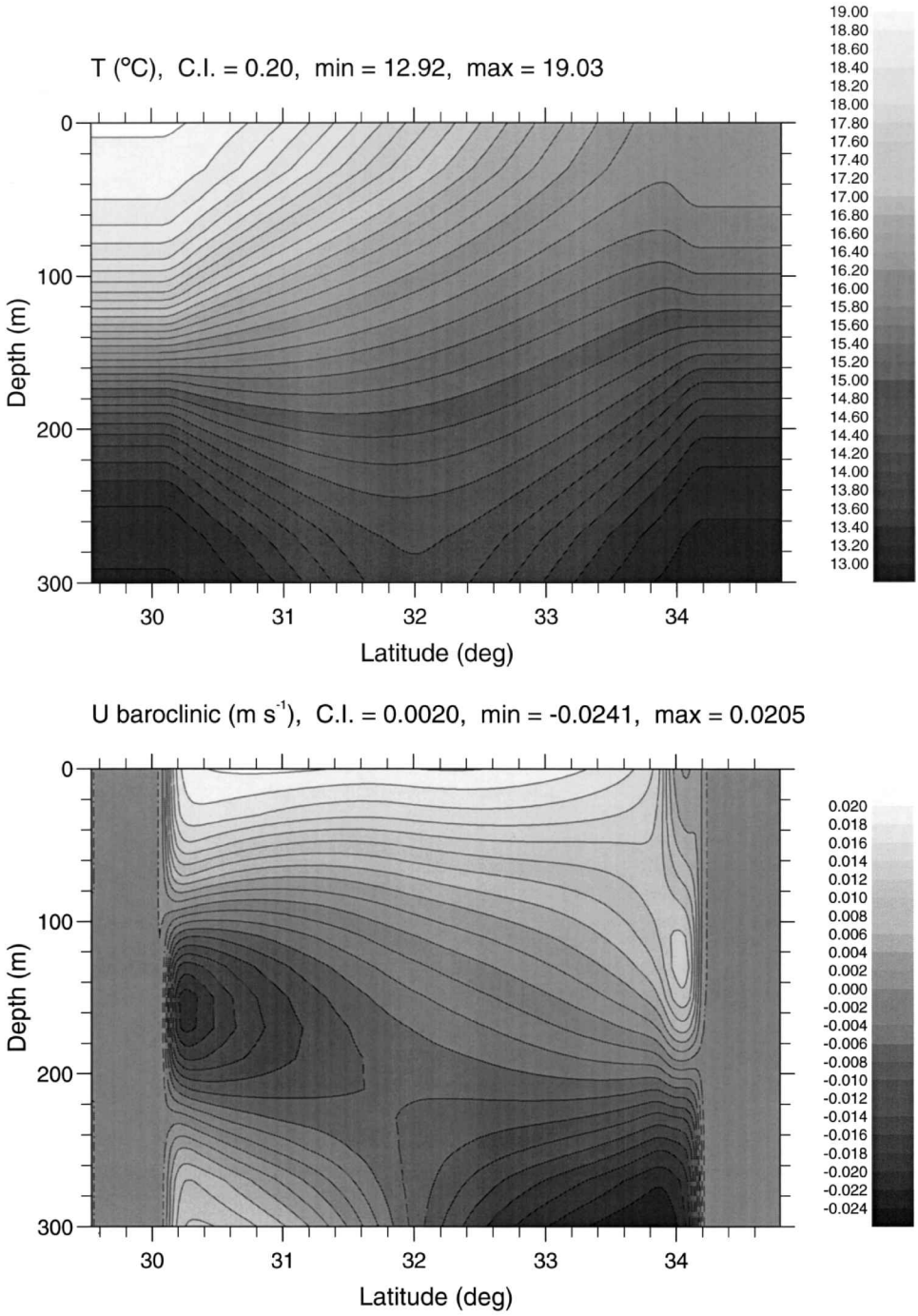

Figure 8. As for Figure 7, but using a coefficient $A = 3.3$ and the small wavenumber formula. (a) Steady state solution for the temperature field. Contour interval 0.2°C, min/max values 12.92, 19.03°C. (b) The baroclinic part of the zonal velocity. Contour interval 0.002 m s^{-1}; min/max values −0.0241, 0.0205 m s^{-1}; (c) The streamfunction for the bolus transport; contour interval 0.05 m^2 s^{-1}; min/max values −0.29, 0.23 m^2 s^{-1}; (d) Distribution of the eddy diffusivity κ; contour interval 20 m^2 s^{-1}; max value 508 m^2 s^{-1}.

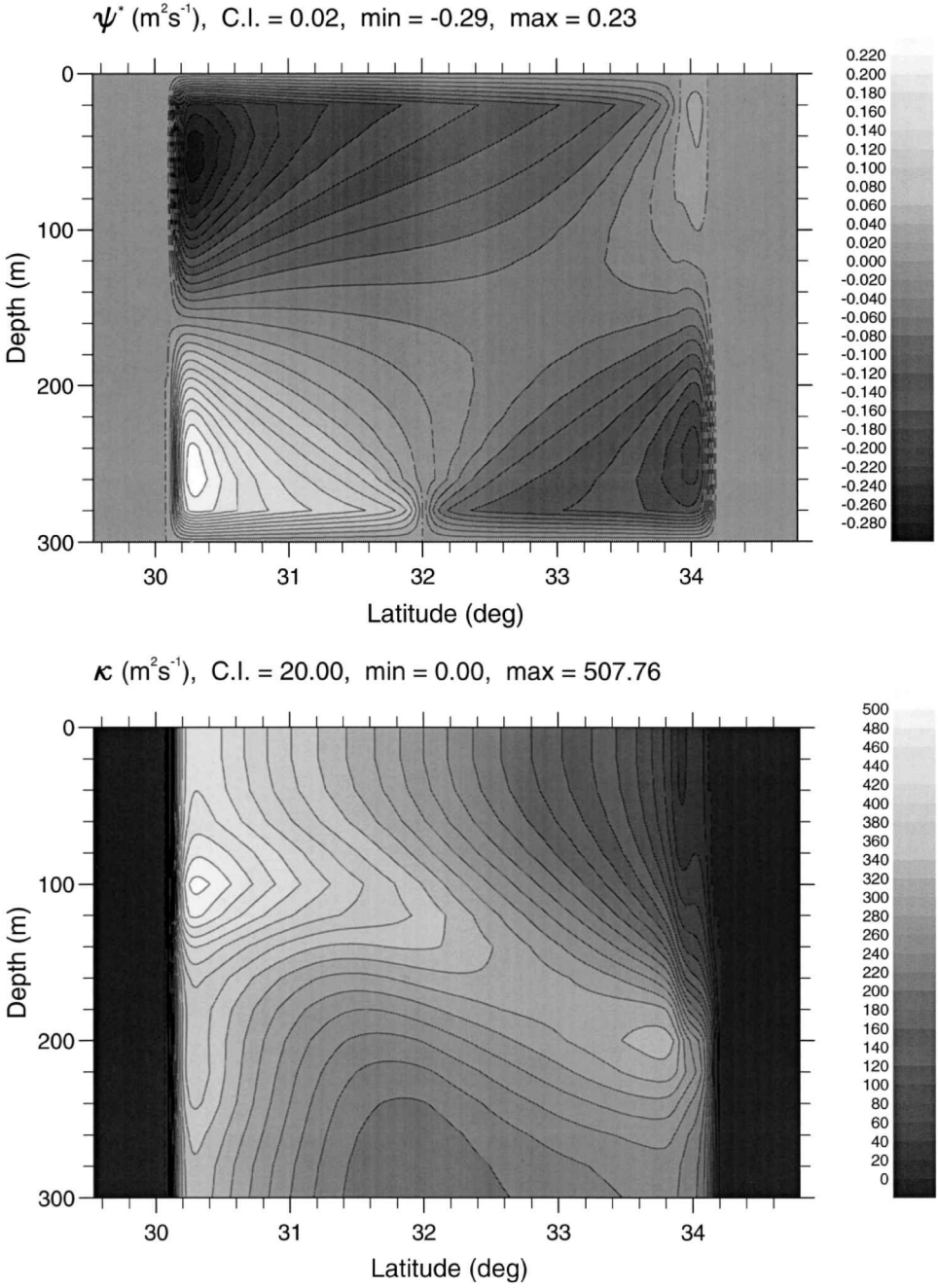

Fig. 8. (Continued)

adjusted field. Thus increasing the magnitude of this constant by 3.3 has increased effective mixing by only 50%, because of the changed density field.

Finally, calculations using two iterations of the iterative procedure, and $A = 3$, give results indistinguishable from those with the small wavenumber and $A = 3.3$.

Thus on this single test the new scheme is almost (numerically) as good as a tuned GM scheme, and visually somewhat superior. Default values of the one adjustable parameter give reasonable fits without tuning, and a tuned value can reproduce both the long-term 3D mean as well as the behavior of the initial slump of the narrow jet. The channel experiment here was unable to differentiate decisively between the iterative and linear schemes.

4. The bolus transport

The previous section compared the predictions of the parameterizations in a two-dimensional model with the time and space averages of the three-dimensional channel model. The process can usefully be inverted, by comparing the bolus transports in the three-dimensional model directly with those estimated from the parameterizations.

Computation of bolus transports is properly carried out by averaging on density surfaces, although there are approximate (quasi-geostrophic) ways to avoid this in layer models (McDougall and McIntosh, 1996; Rix and Willebrand, 1996; Treguier *et al.,* 1997). In Treguier's (1998) channel model, the quasi-geostrophic approximation worked well in comparison with the full averaging approach. Here we only consider the full averaging approach; but the computation needs care. To begin with, although parameterizations ensure that there is no net vertically integrated bolus transport, this need not be the case. Consider the equation for layer thickness

$$z_{\rho t} + \nabla \cdot (\mathbf{u} z_\rho) = F$$

where F represents diapycnal mixing terms (present in the level model used because of diffusions). Taking a vertical integral from lightest (ρ_s) to densest (ρ_b) fluid, the first term vanishes[5] and we have

$$\nabla \cdot \int_{\rho_b}^{\rho_s} \mathbf{u} z_\rho \, d\rho = \int_{\rho_b}^{\rho_s} F \, d\rho.$$

In general, then, there will be some vertically integrated thickness flux due to diabatic effects. If we neglect these, and assume as in K97 that the required solution is of no vertically integrated flux, then we may take a time average to obtain

$$\nabla \cdot \int_{\rho_b}^{\rho_s} \overline{\mathbf{u}' z'_\rho} \, d\rho = -\nabla \cdot \int_{\rho_b}^{\rho_s} \overline{\mathbf{u}}\, \overline{z}_\rho \, d\rho = -\nabla \cdot \int_{-H}^{0} \overline{\mathbf{u}} \, dz = 0.$$

So ignoring diabatic effects, the vertically integrated eddy transport is divergenceless. But in general the transport itself need not be zero, though in the channel model here the net

5. More properly, surface boundary conditions should be included; but the same result holds.

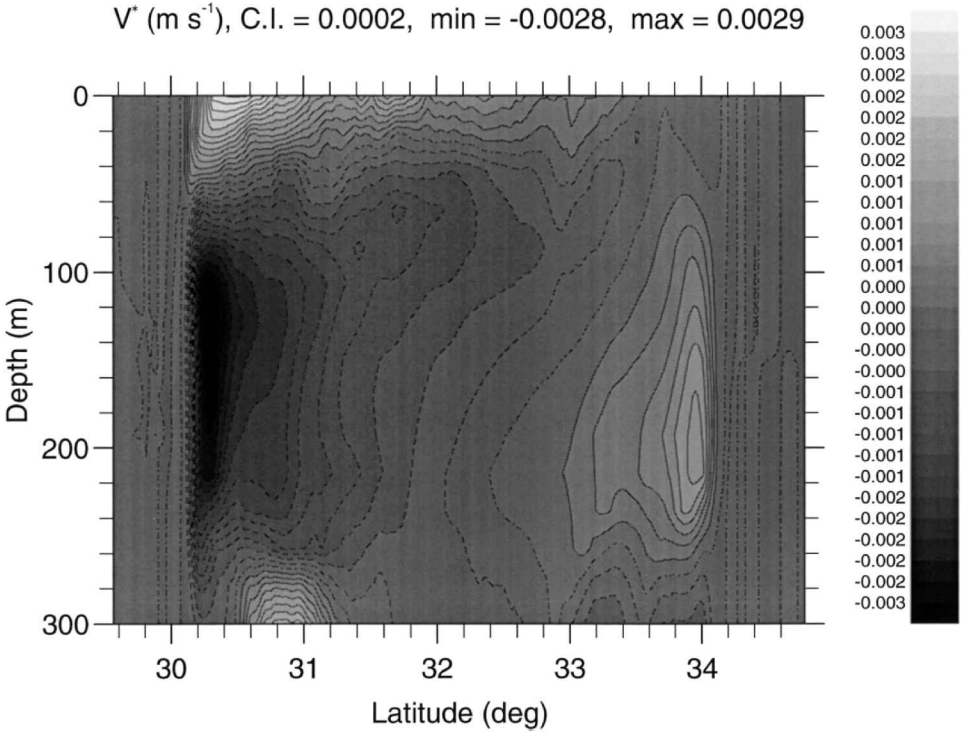

Figure 9. The northward bolus velocity v^* computed from the channel model. Contour interval 0.0002 m s^{-1}; min/max values $-0.0028, 0.0029$ m s^{-1}.

north-south transport should take on values consistent only with diffusive effects in the model. Diabatic effects, as Treguier (1998) notes, need not be small near surface and floor.

Each 10-day snapshot of the channel simulation was converted to density surfaces (here density and temperature are synonymous) before averaging occurred. Perturbation quantities were defined relative to the x- and time-mean within the same period as before. Then $\overline{v'z'_\rho}$ and other similar quantities could be computed. The bolus velocity v^* (still on density surfaces) was then computed from its definition $\overline{v'z'_\rho}/\overline{z}_\rho$, and finally the bolus streamfunction $\psi^*(y, \rho)$ from $\partial\psi^*/\partial\rho = v^*\overline{z}_\rho = \overline{v'z'_\rho}$.

This quantity is easiest displayed for comparison with the bolus streamfunction from the parameterizations on level, rather than density, surfaces. To convert back, the mean density (on level surfaces) was used. Frequently during the run, lateral advection produced situations in which at the surface (floor) lighter (denser) fluid than the mean (level) value at a point occurred, so that in density co-ordinates the bolus velocity, etc. existed but in the mean its value had been lost. This is unavoidable, and makes it difficult to arrive at a bolus streamfunction which truly vanishes at top and bottom.

The results are shown in Figures 9 (for v^*), 10 (for ψ^*), and 11 (for $\overline{\psi} + \psi^*$). No attempt has been made to force the streamfunction to vanish top or bottom. The irregularity

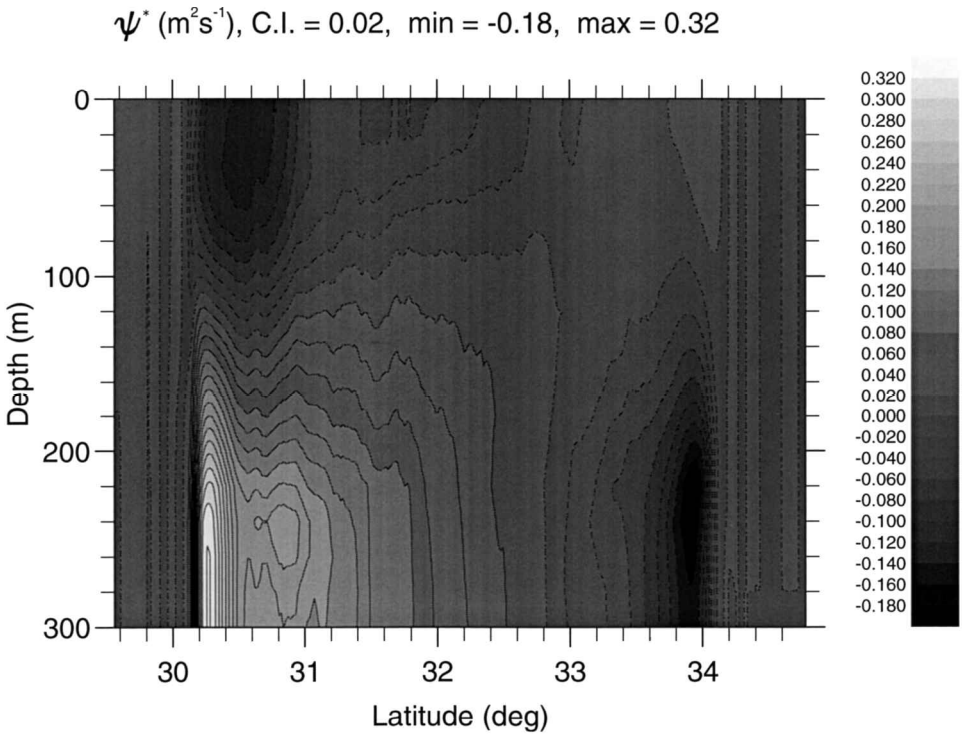

Figure 10. Bolus streamfunction computed from the channel model. Contour interval 0.02 $m^2\ s^{-1}$; min/max values $-0.18, 0.32\ m^2\ s^{-1}$.

demonstrates both that the averaging period is almost certainly too small—one would prefer a period approaching several decades—and that the resolution in density coordinates is poor (the number of density layers was chosen equal to the number of depth layers). The northward bolus velocity, v^*, (Fig. 9) has the expected structure. There is northward transport in the surface layer (moving less dense fluid over more dense fluid) except in the northern corner where the transport is negative. In the middle layers the flux is predominantly southward (dense water under lighter) save again near the northern boundary where the flux is northward. In the deep water, there is northward flux near the southern boundary (again, dense water beneath lighter) and southward flux near the northern boundary (also dense under lighter because of the bowing of the mean isopycnals in Fig. 3).

The bolus streamfunction (Fig. 10) reflects this behavior, although—as discussed above—without vanishing at surface or floor.[6] The *shape* and *amplitude* of the bolus streamfunction are well reproduced by both GM200 and $A = 3.3$, with two large negative regions and one large positive region. The GM streamfunction rather overemphasizes the (in reality small) positive area at the upper northern boundary; in contrast, $A = 3.3$ is much

6. The conversion to depth co-ordinates means that delta-function behavior (in the last gridpoint) as expected from parameterizations is not apparent.

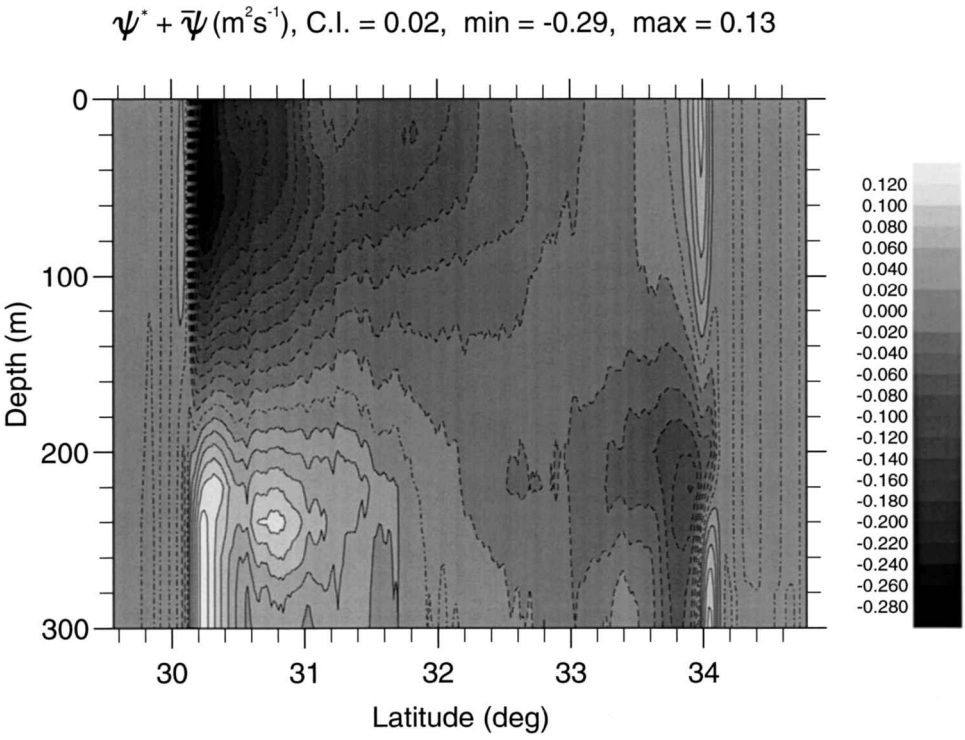

Figure 11. As for Figure 10, but for the total meridional streamfunction $\overline{\psi} + \psi^*$. Contour interval 0.02 $m^2\ s^{-1}$; min/max values $-0.29, 0.13\ m^2\ s^{-1}$.

more accurate. The GM200 minimum is accurate; its maximum is perhaps half the true size. The $A = 3.3$ minimum is 50% too large in amplitude, and its maximum 50% too large.

A similar picture occurs with the total streamfunction (Fig. 11); we compare this also with the parameterization for completeness. The picture remains similar, with a small increase in the positive region at the upper northern boundary; the other three areas of large streamfunction are qualitatively unchanged. Comparing extrema, the GM200 minimum is now 50% too small, with a reasonably accurate maximum; the $A = 3.3$ minimum is accurate, and its maximum 50% too small.

Both parameterizations have thus performed well in reproducing the bolus transport; qualitatively the $A = 3.3$ case would be preferred on shape grounds.

The diffusivity acting in the channel model can also be computed using the definition of v^*. Figure 12 shows contours of κ, although its values are difficult to contour. Solving for κ involves a division, and the denominator changes sign in several locations in the interior of the basin. In such places κ is infinite, and furthermore has sign changes on either side (Treguier, 1998, reports similar difficulties). Nonetheless, these areas are small: over the vast majority of the cross-section, κ is positive and less than 500 $m^2\ s^{-1}$, and the contouring in Figure 12 has been chosen to reflect this. Figure 12 shows that downgradient fluxes of

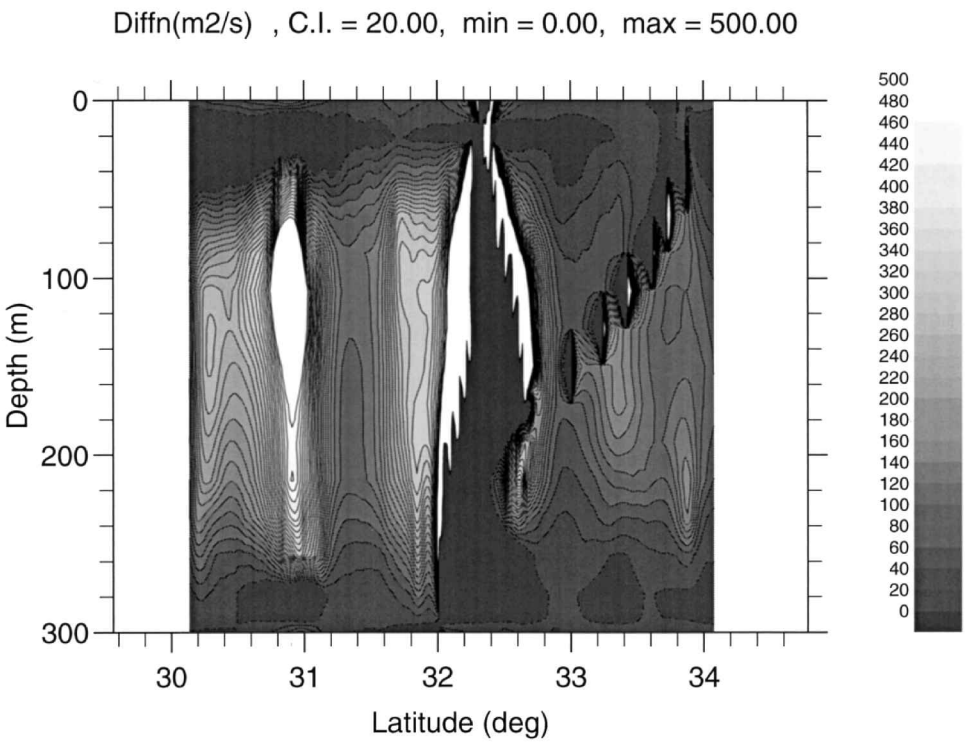

Figure 12. The diffusivity κ computed from the northward bolus velocity v^* in the channel model. Contour interval 20 $m^2\ s^{-1}$. Values above 500 $m^2\ s^{-1}$ are not contoured. Note the existence of subsurface maxima everywhere, and small diffusivities at surface and floor.

potential vorticity occur almost everywhere in the model. The diffusivity is highest, furthermore, at mid-depths as predicted by the parameterization, in agreement with Treguier's (1998) findings, and there are—also as predicted—minima in κ at surface and floor. Because of the areas of large values, no attempt has been made at a quantitative comparison. However, comparison with Figure 8d shows that the subsurface maxima occur in approximately the same vertical positions in both the observed and parameterized diffusivities: the depth of the maximum lies around 100 m at the south, remains at or around that depth across half the basin, then slopes downward to around 200 m at the northern boundary. Weakest values occur in mid-basin in both cases.

5. Conclusions

This paper tests the K97 parameterization scheme, comparing it with Gent and McWilliams (1990) using an eddy-resolving channel model. The barotropic flow is not accurately reproduced by any two-dimensional scheme used here, since no parameterization was included for the Reynolds' stress terms in the momentum equations (by choice). However, the new scheme performs well even with the default-adjustable coefficient set to

unity, though values of order 3 behave better. No version of the new scheme gave as accurate values as a tuned Gent and McWilliams scheme, although the differences are minimal; note that the tuning necessary in the GM scheme involved a rather lower coefficient than would normally be employed. The new scheme was able to reproduce both the long term APE change as well as the initial change due to the slumping of the narrow front. The only adjustable parameter in the new scheme is formally of order unity, which possesses advantages when varying scales are involved.

Both schemes reproduced the bolus streamfunction reasonably well, though the new scheme had a more accurate representation of the shape. Although diagnosed values of diffusivity had small regions of very large values, the general structure of the diffusivity agreed with the new parameterization (and with Treguier's 1998 results), with minimum values at surface and floor, and subsurface maxima.

No test was made here of the more complicated three-dimensional aspects of the parameterization; these will be described in a later paper.

Acknowledgments. This work was partially supported by agreement no. Met2a/0665 from the Hadley Centre. Many colleagues discussed this topic in detail with me and helped to get the ideas in order, especially Mei-Man Lee, George Nurser and Anne-Marie Treguier. Jin Zhang and Jeff Blundell produced much of the numerics in Section 3.

APPENDIX

Numerical issues

For the channel model considered here, the matrix $\mathbf{A}$ is unity and only the diffusivity κ and bolus velocities v^* and w^* need be computed. We take a channel model with variables on a B-grid as in the MOMA version of the GFDL Modular Ocean Model (Webb, 1996; Pacanowski, 1995; cf. Fig. 13) and suppress variation in the east-west direction. The time-stepping algorithm is standard. At each time step, κ can be computed by either of the methods above. At each north-south location, the inner integral in (67)—equation numbers refer to K97—or the simpler integrals in (51), are computed at velocity points by a trapezoidal integration scheme. When c is known, the outer integral (55) or (67) is computed to give the shape of κ at each velocity point, again by a trapezoidal integration. The diffusivity is then computed from (64), using unity for the arbitrary scaling factor to reduce (to zero) the number of arbitrary constants. If κ should be negative anywhere—which it formally can be using the linear approximation—it is set to zero.

Eq. (39) is then used to obtain the northward bolus velocity v^*. (We ignore $\mathbf{A}$ in what follows; u^* is treated similarly.) First the isopycnal slope $S = \rho_y/\rho_z$ is computed at two-dimensional streamfunction points (these are locations for the vertical velocity for the velocity time-stepping calculation), which is the natural location. The slope S can be set to zero on vertical boundaries (or alternatively v^* simply defined to vanish). Interior values of v^* are then straightforwardly computed from (39), since the diffusion κ and $\partial S/\partial z$ are both naturally evaluated at velocity points. Top and bottom grid point values of v^* must include the delta-function behavior. To obtain this, integrate (39) from grid point 1 (in Fig. 13) to

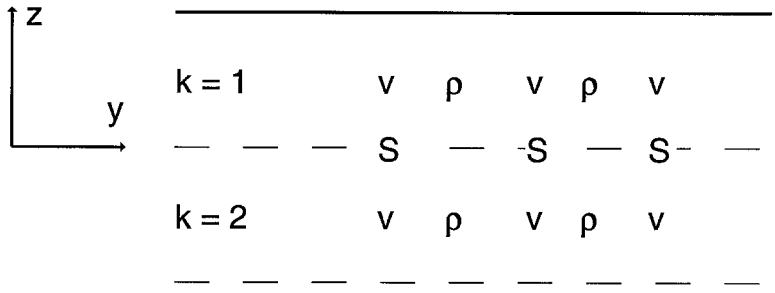

Figure 13. A schematic of the vertical B-grid used in the text.

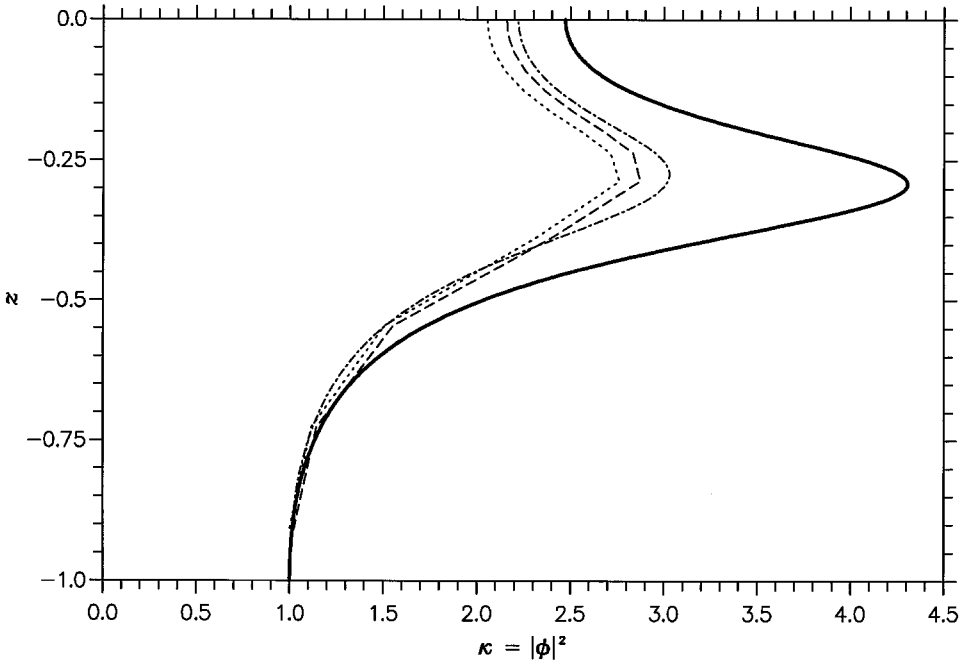

Figure 14. Errors produced by discretization in the estimates of κ. The solution is that for Figure 3 (b) in K97. The bold line shows the fastest growing mode solution; the other three lines show second iterates of the approximate solution (each is close to the appropriate infinitely iterated solution). The dash-dotted line is the second iterate computed exactly (actually with a very large number of gridpoints). The remaining solutions use 16 gridpoints at depths at alternate NODC standard levels; they are chosen to emulate typical g.c.m. grid spacing. The dotted line shows the solution where the inner integral in (67; K97 is evaluated at *w* points; the dashed line where it is evaluated at *u* points.

the surface over the local grid thickness Δz, and use the fact that κ_z vanishes at the surface:

$$\int_{-\Delta z}^{0} v^* \, dz = \kappa(S_0 - S_1) + \frac{\beta}{f}\kappa\Delta z - \kappa S_0 = -\kappa S_1 + \frac{\beta}{f}\kappa\Delta z$$

so that S_0, the surface slope, does not need to be known (and can be set to zero for computational convenience). Then

$$v_1^* = \frac{1}{\Delta z}\int_{-\Delta z}^{0} v^* \, dz = -\frac{\kappa S_1}{\Delta z} + \frac{\beta}{f}\kappa$$

is the effective bolus velocity in the top grid point. Similarly, at the bottom internal point N, say, $v_N^* = \kappa S_{N-1}/\Delta z + \beta\kappa/f$.

This formulation, with a fully accurate computation of κ together with fine vertical resolution, would be sufficient to ensure the vanishing of the vertical integral of v^* because the necessary condition is approximately satisfied. In general because of numerical errors this will not occur; so that w^* can be computed correctly, the vertical average of v^* is subtracted from v^* before w^* is calculated from the divergence equation.

Numerical errors, as usual, affect eigenvectors worse than eigenvalues. Figure 14 shows an example using a grid spacing of 16 alternate NODC standard levels, and two iterations of the iterative approach. Reducing the grid points to 8 doubles the error in the κ profile, but has only an $O(\Delta z^2)$ effect on c and k. One can choose to evaluate the inner integral in (67) in two ways: at velocity depths, by a simple trapezoidal or two half-slab integrations, or at w depths, by a slab integration. Consistently, the velocity level calculation is slightly closer to the exact solution, and it is recommended that this method be employed. Precisely which of the four possible combinations of integration methods for the pair of integrals in (67) is most accurate numerically appears to depend on resolution; for a uniform grid spacing, all are equivalent, of course.

For numerical stability, it is necessary to calculate the bolus velocity terms at the lagged timestep when a leapfrog time integration method is used (note that in the GM scheme both bolus velocity and advected temperature must be lagged).

In the fully three-dimensional case, computations are similar, though in addition the angle θ must also be computed locally.

REFERENCES

Farrow, D. E. and D. P. Stevens. 1995. A new tracer advection scheme for Bryan and Cox type ocean general circulation models. J. Phys. Oceanogr., *25,* 1731–1741.

Gent, P. R. and J. C. McWilliams. 1990. Isopycnal mixing in ocean circulation models. J. Phys. Oceanogr., *20,* 150–155.

——1996. Eliassen-Palm fluxes and the momentum equation in non-eddy resolving ocean circulation models. J. Phys. Oceanogr., *26,* 2539–2546.

Gent, P. R., J. Willebrand, T. J. McDougall and J. C. McWilliams. 1995. Parameterizing eddy-induced transports in ocean circulation models. J. Phys. Oceanogr., *25,* 463–474.

Harrison, D. E. 1978. On the diffusion parameterization of mesoscale eddy effects from a numerical ocean experiment. J. Phys. Oceanogr., *8,* 913–918.

Killworth, P. D. 1997. On the parameterization of eddy transfer. Part I: Theory. J. Mar. Res., *55,* 1171–1197.

Lee, M.-M. and H. Leach. 1996. Eliassen-Palm flux and eddy potential vorticity flux for a nonquasigeostrophic time-mean flow. J. Phys. Oceanogr., *26,* 1304–1319.

Marshall, J. C. 1981. On the parameterization of geostrophic eddies in the ocean. J. Phys. Oceanogr., *11,* 257–271.

McDougall, T. J. and P. C. McIntosh. 1996. The temporal-residual-mean velocity. Part I: Derivation and the scalar conservation. J. Phys. Oceanogr., *26,* 2653–2665.

Pacanowski, R. C. 1995. MOM 2 documentation, user's guide and reference manual. GFDL Ocean Group Technical Report No. 3. Geophysical Fluid Dynamics Laboratory/NOAA, Princeton University, Princeton, New Jersey, 232 pp.

Rix, N. H. and J. Willebrand. 1996. Parameterization of mesoscale eddies as inferred from a high-resolution circulation model. J. Phys. Oceanogr., *26,* 2281–2285.

Samelson, R. M. 1993. Linear instability of a mixed-layer front. J. Geophys. Res., *98,* 10195–10204.

Simmons, A. J. and B. J. Hoskins. 1978. The life cycle of some nonlinear baroclinic waves. J. Atmos. Sci., *35,* 414–432.

Treguier, A. M. 1998. Evaluating eddy mixing coefficients from eddy resolving ocean models: a case study. J. Phys. Oceanogr., (submitted).

Treguier, A. M., I. M. Held and V. D. Larichev. 1997. On the parameterization of quasi-geostrophic eddies in primitive equation ocean models. J. Phys. Oceanogr., *27,* 567–580.

Visbeck, M., J. Marshall, T. Haine and M. Spall. 1997. On the specification of eddy transfer coefficients in coarse resolution ocean circulation models. J. Phys. Oceanogr., *27,* 381–402.

Webb, D. J. 1996. An ocean model code for array processor computers. Computers and Geosciences, *22,* 569–578.

Welander, P. 1973. Lateral friction in the ocean as an effect of potential vorticity mixing. Geophys. Fluid Dyn., *5,* 173–189.

Received: *27 April, 1997;* revised: *23 October, 1997.*